Article

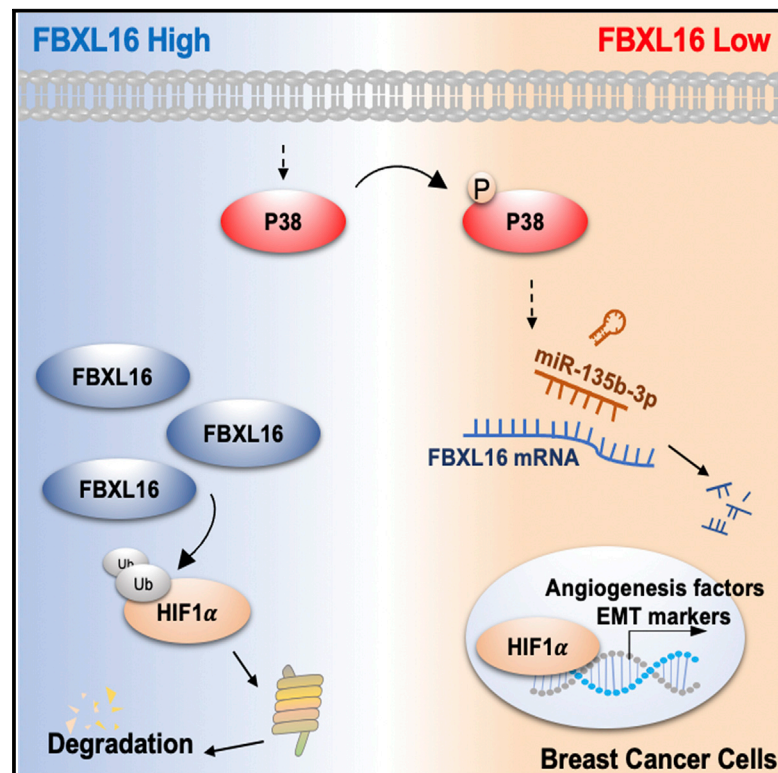# Suppression of breast cancer progression by FBXL16 via oxygen-independent regulation of HIF1α stability

Graphical abstract

Highlights

- Expression of FBXL16 is downregulated by the p38/miR-135b-3p axis in TNBCs

- Loss of FBXL16 expression induces poor clinical outcomes in patients with breast cancer

- FBXL16 binds to HIF1a for ubiquitination under both normoxic and hypoxic conditions

- Modulating the expression of FBXL16 can attenuate breast cancer progression

Authors

Yeon-Ju Kim, Yi Zhao, Jae Kyung Myung, Joo Mi Yi, Min-Jung Kim, Su-Jae Lee

Correspondence

sj0420@hanyang.ac.kr

In brief

Kim et al. find that expression of FBXL16 is downregulated in triple-negative breast cancers. FBXL16 acts as a tumor suppressor in TNBCs. FBXL16 directly binds to HIF1α and induces its ubiquitination and degradation, regardless of the tumor microenvironment. Targeting of FBXL16 expression may offer a therapeutic strategy for treatment of patients with breast cancer.

CellPress

Article

Suppression of breast cancer progression by FBXL16 via oxygen-independent regulation of HIF1α stability

Yeon-Ju Kim,[1,5] Yi Zhao,[1,5] Jae Kyung Myung,[2] Joo Mi Yi,[3] Min-Jung Kim,[4] and Su-Jae Lee[1,6,*]

[1]Department of Life Science, Research Institute for Natural Sciences, Hanyang University, Seoul 04763, Republic of Korea
[2]Department of Pathology, Hanyang University Medical Center, 222-1, Wangsimni-ro, Seongdong-gu, Seoul, Republic of Korea
[3]Department of Microbiology and Immunology, College of Medicine, Inje University, Busan 47392, South Korea
[4]Laboratory of Radiation Exposure and Therapeutics, National Radiation Emergency Medical Center, Korea Institute of Radiological and Medical Sciences, Seoul, South Korea
[5]These authors contributed equally
[6]Lead contact
*Correspondence: sj0420@hanyang.ac.kr
https://doi.org/10.1016/j.celrep.2021.109996

SUMMARY

Triple-negative breast cancers (TNBCs) are characterized by high rates of recurrence and poor clinical outcomes. Deregulated E3 ligases are involved in breast cancer pathogenesis and progression, but the underlying mechanisms are unclear. Here, we find that F-box and leucine-rich repeat protein 16 (FBXL16) acts as a tumor suppressor in TNBCs. FBXL16 directly binds to HIF1α and induces its ubiquitination and degradation, regardless of the tumor microenvironment, resulting in blockade of the HIF1α-mediated epithelial-mesenchymal transition (EMT) and angiogenesis features of breast cancer. In TNBCs, FBXL16 expression is downregulated by the p38/miR-135b-3p axis, and loss of FBXL16 expression restores HIF1α-mediated metastatic features of breast cancer. Low expression of FBXL16 is associated with high-grade and lymph node-positive tumors and poor overall survival of breast cancer. Taken together, these findings demonstrate that modulation of FBXL16 expression may offer a favorable strategy for treatment of patients with metastatic breast cancer, including TNBCs.

INTRODUCTION

Breast cancer is a frequently diagnosed cancer, and the leading cause of cancer-related death among women worldwide (Torre et al., 2017). Breast cancer has been classified by the presence of hormone receptors, with molecular subtypes being based on the tumor cell expression of estrogen receptor (ER), progesterone receptor (PR), and epithelial growth factor receptor 2 (HER2) (Vuong et al., 2014). Triple-negative breast cancers (TNBCs), in which expression of all three receptors is absent, have a worse prognosis, are more aggressive, and metastasize more readily than other subtypes of breast cancer, which limits therapeutic options (Dent et al., 2007). Therefore, new therapeutic strategies for treatment of TNBC sare urgently needed.

The ubiquitin-proteasome system (UPS) is a critical protein degradation system that plays important roles in regulating cellular protein levels, activity, and location (Yang et al., 2009). Ubiquitination is catalyzed by E1 (ubiquitin-activating enzyme), E2 (ubiquitin-conjugating enzyme), and E3 (ubiquitin protein ligase), which recognizes target proteins and ultimately determines the target of the ubiquitination machinery. E3 ligases can be categorized into four families: RING-finger, HECT, U-box, and PHD finger (Bai et al., 1996). Of these, the largest and most well-studied family are RING-finger E3 ligases, which include ligases such as the anaphase-promoting complex (APC), and the SCF complex (Skp1-Cullin-F-box protein complex). The SCF complex consists of SKP1, CUL1, and F-box proteins (FBPs), which contain a substrate-binding domain that confers target specificity to the complex (Skowyra et al., 1997; Wang et al., 2014). Moreover, FBPs are involved in development and progression of various cancers (Randle and Laman, 2016). A previous study showed that FBXL16 was upregulated by E2F1 in p16INK4A and p14ARF knockout HeLa cells, and loss of FBXL16 expression promoted cell proliferation (Sato et al., 2010). Furthermore, FBXL16 regulates embryonic stem cell differentiation by binding to protein phosphatase 2A (PP2A), containing a B55 subunit (PP2AB55) (Honarpour et al., 2014). Despite these interesting initial findings about FBXL16 that hint at important functions, the roles and mechanistic functions of FBXL16 in breast cancer are largely unexplored.

The transcriptional regulator hypoxia-inducible factor 1α (HIF1α) is known to be hyperactivated and upregulated in various tumors, either in response to intratumoral hypoxia or independent of hypoxia (Semenza, 2012). Prior studies have reported that HIF1α plays a significant role in regulating tumor angiogenesis, cancer stemness, cell invasion, and migration (Chen et al.,

2014; Lin et al., 2016; Montagner et al., 2012; The Cancer Genome Atlas Network, 2012). Additionally, high expression of HIF1α is correlated with advanced disease and poor patient prognosis (Gilkes et al., 2014; Liu et al., 2015). Hence, targeting signaling pathways related to HIF1α would be a novel and logical therapeutic option in TNBCs.

In this study, we identified that FBXL16 plays a tumor-suppressive role in breast cancer progression. Specifically, FBXL16 directly binds to HIF1α to regulate its ubiquitination and degradation, resulting in the attenuation of the HIF1α-mediated EMT and angiogenesis features of breast cancer. Additionally, we also found that FBXL16 expression was inhibited by the p38/miR135b-3p axis in TNBCs, and the loss of FBXL16 expression was correlated with poor clinical outcomes. Therefore, our results further suggest that modulation of FBXL16 expression in TNBCs may provide a rewarding strategy for TNBC treatment.

RESULTS

Low expression of FBXL16 in TNBCs and association with poor clinical prognosis

To explore possible tumor suppression activity of F-box proteins in breast cancer, we screened a total of 69 F-box proteins using the TCGA breast cancer database. We list here the top five genes whose expression was higher in luminal type rather than basal type breast cancer, with FBXL16 having the highest expression level in luminal type breast cancer compared to other F-box proteins (Figure 1A). The METABRIC, TCGA, GSE1456, and GSE19615 breast cancer databases also showed results consistent with our observation (Figures 1B–1D). Additionally, heatmap analysis showed that FBXL16 showed the lowest expression level among these FBPs in TNBC cell lines using the GSE41313 database (Figure 1E). To verify these findings, we performed quantitative real-time PCR and western blotting analysis using different subtypes of breast cancer cell lines. We found that FBXL16 expression was lower in the TNBC subtype than in other subtypes of breast cancer, at both the mRNA and protein levels (Figure 1F). Furthermore, immunohistochemical staining revealed that FBXL16 showed a lower expression level in TNBC patient tissues compared to those from patients with ER/PR[+] and HER2^{+} cancers (Figure 1G). Moreover, lymph node-positive breast cancer patients also showed a low expression compared to negative patients (Figure 1H). Kaplan-Meier survival analysis using the GSE19615, GSE21653, and GSE42568 databases and tissue array staining showed that an elevated level of FBXL16 expression correlated with a higher survival rate in patients independent of the status of breast cancer types and lymph nodes (Figure 1I–1L). Taken together, these data suggest that downregulation of FBXL16 expression is associated with metastatic breast cancer and poor clinical outcomes.

FBXL16 expression suppresses EMT and angiogenesis in breast cancer

To investigate the function of FBXL16 in breast cancer, GSEA analysis was performed using GSE4922 database to identify the characteristics of breast cancer that were regulated by FBXL16 expression. We found that high expression of FBXL16 negatively regulated the EMT and angiogenesis phenotypes of

breast cancer (Figures 2A and 2B). To confirm these findings, we overexpressed FBXL16 in basal type MDA-MB231 breast cancer cells or knocked down FBXL16 in MCF7 luminal breast cancer cells using small interfering RNA (siRNA) against FBXL16. Invasion and migration assays showed the potentials for cell invasion and migration were inhibited, and the expression of EMT markers and regulators were also decreased, as assessed by quantitative real-time PCR, western blotting, and immunocytochemistry staining analysis in FBXL16-overexpressing MDA-MB231 cells. The reverse results were observed in FBXL16-silenced MCF7 cells (Figures 2C and 2D; Figures S1A–S1D). HUVEC tube formation was decreased, as evidenced by the significantly reduced tube length and total number of branch points compared to the control group as well as the expression of angiogenesis markers after overexpression of FBXL16 in MDA-MB231 cells (Figures 2E–2G; Figures S1E–S1G). To confirm whether these in vitro findings could also be observed in vivo, we injected control and FBXL16-overexpressing lung-metastasized MDA-MB231 (LM1) cells into the fat pad of female NOD/SCID mice (n = 6 in each group). Before the mice experiment, we assessed the LM1-FBXL16 overexpression efficiency compared to the endogenous HIF1α expression in MCF7 cells by western blotting analysis (Figure 2H). Lung metastatic foci, tumor volumes, and weight showed a significant decrease in LM1-FBXL16 groups, with a decrease in EMT and angiogenesis markers and regulator expression compared to the control groups (Figures 2I–2N; Figures S1H–S1J). Furthermore, the expression of proliferation marker Ki67 was also inhibited in FBXL16-overexpressing groups as assessed by IHC staining analysis (Figure S1K), which further supported the interpretation that FBXL16 can influence tumor growth. Overall, the expression of FBXL16 was linked to EMT and the angiogenesis potential of breast cancer, both in vitro and in vivo.

HIF1α is a direct target of FBXL16 for proteasome degradation in breast cancer

To determine how FBXL16 can downregulate EMT and angiogenesis in breast cancer, we did GSEA analysis using the data from GSE3494 and GSE18864. We found that the hallmarks of EMT, angiogenesis, hypoxia, and the HIF1α signaling pathway always showed an obvious negative correlation with FBXL16 expression in breast cancer (Figure 3A). Previous studies also reported that HIF1α played a significant role in regulating EMT and angiogenesis in cancers (Zhang et al., 2016). When we overexpressed FBXL16, the HIF1α protein expression level was decreased, while there was no significant difference in the mRNA expression level in MDA-MB231 cells. The opposite results were observed in FBXL16-silenced MCF7 cells (Figures 3B and 3C). Therefore, we hypothesized that FBXL16 maybe directly bind to HIF1α to regulate its stabilization in breast cancer. To extend our hypothesis, we performed a CHX pulse chase assay and found that the protein stability of HIF1α quickly decreased depending on FBXL16 overexpression in MDA-MB231 cells compared to the control group (Figure 3D). Subsequently, we transfected FLAG-FBXL16 and HA- HIF1α vectors together or alone with His-Ub vectors into HEK293T cells to check the ubiquitination of HIF1α. The cells were treated for 6 h with MG132 to inhibit protein degradation before being
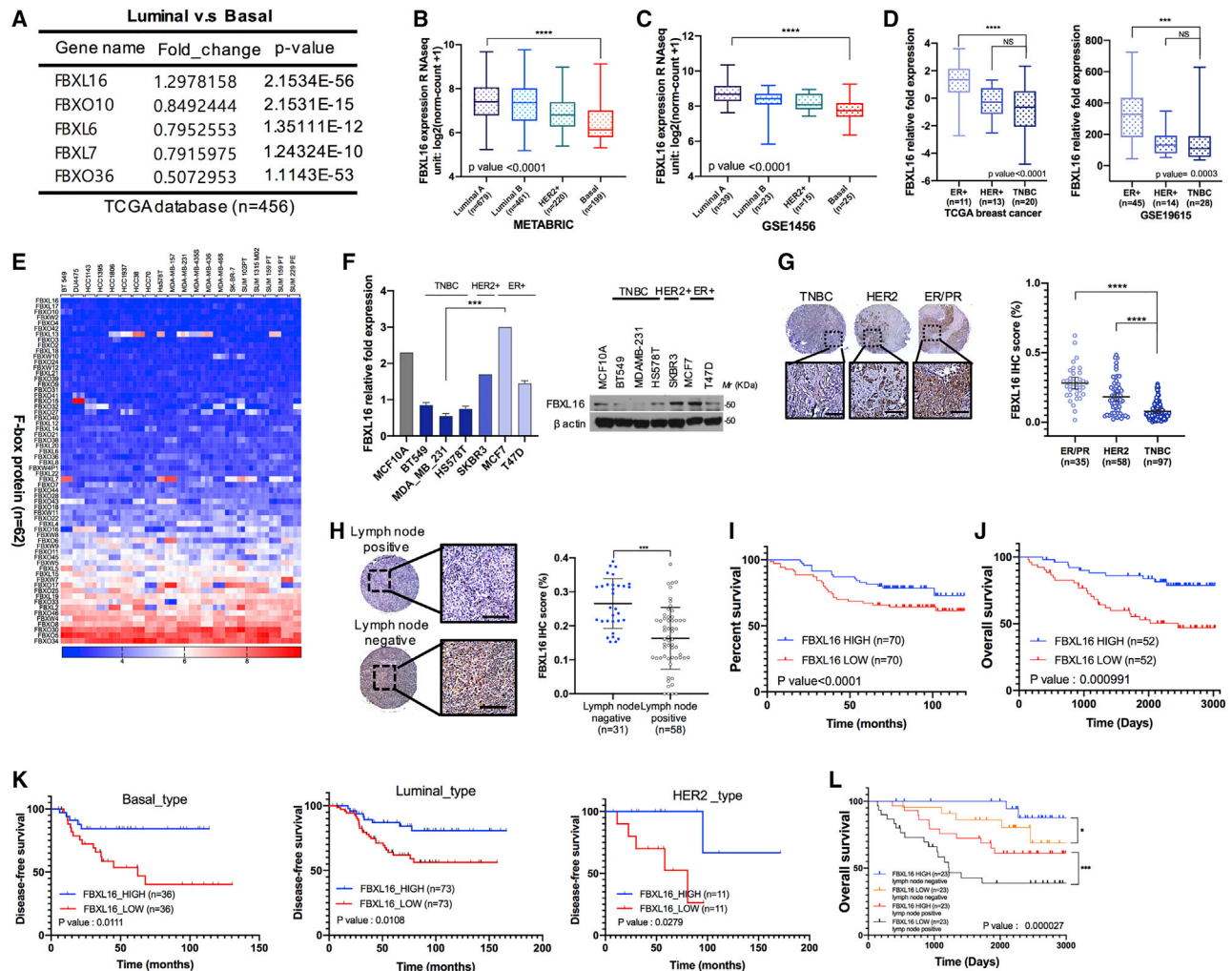
Figure 1. FBXL16 is expressed at a high level in luminal type breast cancer

(A) E3 ligase expression data in basal and luminal types of breast cancer extracted from the TCGA breast cancer database, ranked by their average score calculated for patient gene expression (n = 456). Each ranking is the fold change for expression in luminal type versus basal type breast cancer.

(B and C) Analysis of FBXL16 expression using the microarray data from GEO dataset (GSE1456), and METABRIC breast cancer database.

(D) Analysis of FBXL16 expression depending on the classification analysis of breast cancer by microarray data from TCGA database and GEO dataset (GSE19615).

(E) Heatmap showing the expression of F-box proteins in TNBCs using the GEO breast cancer cell line dataset (GSE41313, n = 150). Blue and orange indicate downregulation and upregulation, respectively.

(F) Quantitative real-time PCR (left) and western blotting (right) analysis of FBXL16 expression levels in different types of breast cancer.

(G) Representative IHC images of FBXL16 staining protein in ER/PR, HER$^+$, and TNBC subtypes of breast cancer (right). The graph shows the proportion of FBXL16 expression (left).

(H) Comparison by IHC staining of FBXL16 expression levels in lymph node-metastasis patient tissues and metastasis-free patient tissues (right). The proportion of FBXL16 expression is shown in the graph (left).

(I–K) Kaplan-Meier survival analysis shows that low expression of FBXL16 is associated with a poor patient survival rate in breast cancer patients independent on the subtypes of breast cancer using the data from the breast cancer tissue assay (I) and public GEO databases (GSE42568 and GSE21653)

(L) Kaplan-Meier survival analysis shows that high levels of FBXL16 expression along with lymph node metastasis patients were associated with higher survival rates of patients with breast cancer. Values in the graph represent the means ± SD (n = 3). **p < 0.01, ***p < 0.001; n.s., not significant. All data were statistically analyzed by a t test (95% confidence interval).

harvested for subsequent experiments. The ubiquitination of FBXL16 was increased after co-overexpression of FBXL16 and HIF1α vectors compared to overexpressed HIF1α vector alone in His-Ub-overexpressing HEK293T cells (Figure 3E). The immunoprecipitation assay was performed to measure the endoge-

nous protein interaction between FBXL16 and HIF1α in MCF7 cells (Figure 3F). Then we transfected FBXL16-overexpressing vector into MDA-MB231 cells, co-immunoprecipitation (coIP) assays showed an interaction between FBXL16 and HIF1α, the consistent results were also observed in HEK293T cells with
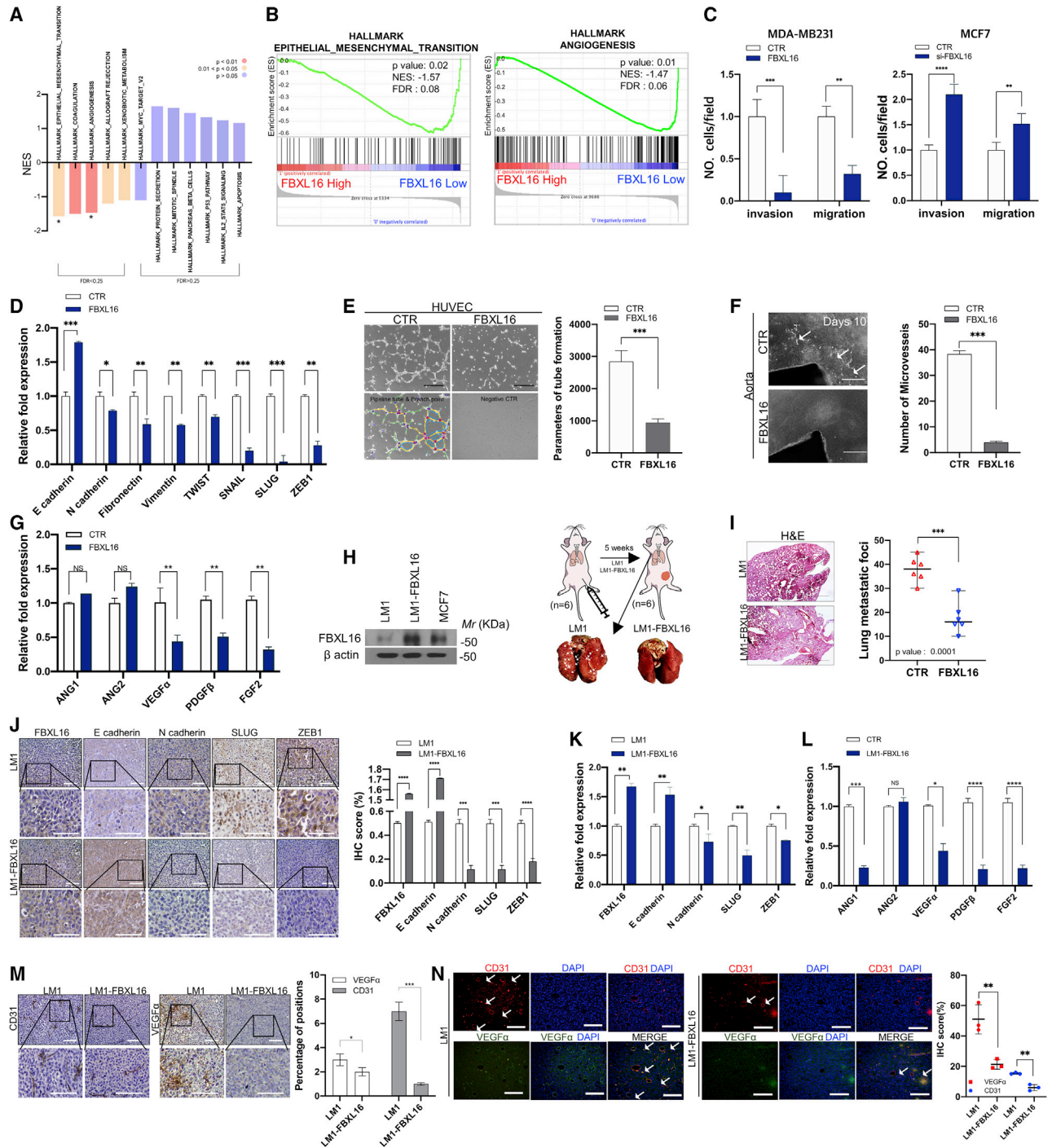

Figure 2. FBXL16 suppresses EMT and angiogenesis in breast cancer

(A and B) GSEA analysis of the enrichment of the EMT and angiogenesis hallmarks using the data from GEO dataset (GSE4922).

(C) Invasion and migration assays were performed using the FBXL16-overexpressing MDA-MB231 cells (left) and FBXL16-silenced MCF7 cells (right).

(D) Quantitative real-time PCR expression analysis of EMT markers and regulators in MDA-MB231 transfected with FBXL16 overexpression vector.

(E) Percentage of HUVEC tube-formation ability of FBXL16-infected cells (left) and representative images of the HUVEC tube-formation assay after restoration of FBXL16 expression in MDA-MB231 cells (right). The values were calculated by NIH ImageJ software (p < 0.001, Student's t test).

(F) Images effects of FBXL16 on the microvessel outgrowth of the aortic ring assay (white arrows) and the ring that was embedded in a matrigel for 10 days (left). Quantification of microvessel formation by calculated image analysis of aortic ring assay (right) is shown.

(G) Quantitative real-time PCR expression analysis of angiogenesis markers using the FBXL16-overexpressing MDA-MB231 cells.

(legend continued on next page)

co-overexpression of FBXL16 and HIF1α (Figures 3G and 3H). Additionally, the GST-pull down and *in situ* assays also showed that HIF1α was a direct target of FBXL16 (Figures 3I and 3J). Western blotting and IHC staining analysis revealed that overexpression of FBXL16 decreased HIF1α protein expression levels in mouse tissues, while there was no change at mRNA expression (Figures S2A and S2B). Next, we performed western blotting analysis using the HIF1α-overexpressing MCF7 cells with or without knockdown of FBXL16. We found HIF1α expression was suppressed by FBXL16, which cannot induce an increase by itself (Figure S2C). Furthermore, our data showed that the invasive/migratory and tube-formation abilities of cells were inhibited when we overexpressed FBXL16 alone, while their aggressive abilities were rescued by overexpression of FBXL16 together with HIF1α in MDA-MB231 cells (Figures 3K and 3L). Similar results were observed for the expression of EMT and angiogenesis markers and regulators at both the mRNA and protein-expression level (Figures 3M and 3N; Figures S2D–S2F). Additionally, we also used the ER+ (MCF7 and T47D) and HER2+ (MDA-MB453 and SKBR3) types of breast cancer cell lines to measure the EMT signature genes expression with blocking FBXL16 expression alone or together with HIF1α, and then we found the elevated EMT markers and regulators expression can be destroyed by silencing endogenous HIF1α expression both in ER+ and HER2+ types of breast cancer cells (Figures S2G–S2J). Taken together, we infer that FBXL16 directly binds to HIF1α to regulate its ubiquitination and degradation and then regulates EMT and angiogenesis in breast cancer.

FBXL16 regulates HIF1α ubiquitination and degradation regardless of oxygen conditions in breast cancer

Extensive studies have demonstrated that HIF1α protein degradation is regulated by oxygen-dependent prolyl hydroxylation (Masson et al., 2001; Serra-Pérez et al., 2010). The von-Hippel Lindau tumor suppressor (VHL) functions as a master regulator of HIF1α protein activity by targeting the hydroxylated HIF1α for proteasomal degradation under normoxic conditions (Jaakkola et al., 2001). To explore the role of VHL and FBXL16 in regulating stability of HIF1α in breast cancer, we first compared the expression levels of VHL and FBXL16 in different breast cancer subtypes using METABTIC, GSE41313, UCSC hub breast cancer databases. We found that FBXL16 was highly expressed in the luminal type of breast cancer compared to other types of breast cancer, but there was no significant difference in the expression of VHL in the ER/PR+, HER2+, or TNBC subtypes (Figure 4A). Then the degradation of HIF1α was measured after treatment with CHX (100 μg/mL) at the indicated time points. We found that overexpression of FBXL16 or VHL together with HIF1α

increased the speed of HIF1α protein degradation compared to overexpressing HIF1α alone in HEK293T cells (Figure 4B). VHL has been reported to not bind to HIF1α under hypoxic conditions, and our data are consistent with this finding using HIF1α-overexpressing HEK293T cells treated with cobalt chloride (CoCl$_2$), which is a well-known hypoxia mimetic that induces hypoxia-like responses (Tripathi et al., 2019) (Figure 4C). VHL-mediated polyubiquitination of HIF1α requires hydroxylation of specific proline residues Pro402 and Pro564 in human HIF1α (Hon et al., 2002). Hence, we examined whether FBXL16 regulates HIF1α ubiquitination and degradation via the same proline residues. We transfected the HIF1α P402A/P564A mutation vector into CHX-treated cells with or without FBXL16/VHL-overexpressing HEK293T cells. We found that the mutation of the proline residues in HIF1α did not influence the ability of FBXL16 to regulate HIF1α degradation under both normoxic and hypoxic conditions (Figures 4D and 4E). Therefore, FBXL16 regulation of HIF1α stability did not require hydroxylation of specific proline residues Pro402 and Pro564 in human HIF1α. Furthermore, we also used ER+ and HER2+ breast cancer cell lines to check HIF1α expression when the FBXL16 expression was blocked by siRNA with or without CoCl$_2$ treatment. Then, we found that the HIF1α expression was increased when we knocked down FBXL16 expression both in normoxia and hypoxic conditions independent on the types of breast cancer types (Figures S3A–S3D). To substantiate these findings, the endogenous HIF1α protein expression level was measured in MDA-MB231 breast cancer cells with or without CoCl$_2$ treatment for 24 h. We found that the HIF1α protein expression level was drastically decreased in FBXL16-overexpressing MDA-MB231 cells with or without CoCl$_2$ treatment; however, VHL only decreased HIF1α protein expression in MDA-MB231 cells that were not treated with CoCl$_2$ (Figures 4F and 4G; Figure S3E). Consistent results were also observed in HEK293T cells and MDA-MB231 breast cancer cells cultured in 1% O$_2$ at the indicated time points (Figure S3F). Similar results were also obtained in HIF1α-overexpressed HEK293T cells and HIF1α hydroxylation-deficient (P402A/P564A) HEK293T cells (Figures 4H and 4I; Figures S3G and S3H). CoIP assays showed that both FBXL16 and VHL could interact with HIF1α under normoxic conditions (Figure 4J). Furthermore, only FBXL16 regulated HIF1α protein degradation in HIF1α P402A/P564A-overexpressing HEK293T cells. VHL cannot bind to HIF1α in HIF1α hydroxylation-deficient HEK293T cells (Figures 4K and 4L). Taken together, these results indicate that FBXL16 directly interacts with HIF1α to regulate its ubiquitination and degradation, irrespective of oxygen conditions. Moreover, FBXL16 binds to HIF1α at a different site compared to VHL-mediated ubiquitination of HIF1α in breast cancer.

(H) Western blotting analysis was performed to check the overexpression efficiency of FBXL16 compared with the FBXL16 endogenous expression in MCF7 cell. Schematic of *in vivo* experiments for injection of the mouse fat pad with 1 × 10^6 of control and/or FBXL16-overexpressing LM-1 cells into NOD/SCID mice (n = 6 each group, top) and representative image of lung metastatic nodules (bottom).

(I) H&E staining of spontaneous lung metastasis (left) and quantification of lung metastatic foci with graph (right).

(J) Representative images of IHC staining of EMT markers and regulators (left), and quantification of expression of EMT markers and regulators in primary tumor (right). Mean of three biological replicates is shown.

(K and L) Quantitative real-time PCR expression analysis of EMT and angiogenesis regulators and markers in primary tumor.

(M and N) Representative images of IHC and IF staining of VEGFα and CD31 in primary tumor (left and the graph showing the quantification of staining (right). Three biological replicates were performed. **p < 0.01, ***p < 0.001; n.s., not significant. All data were statistically analyzed by a t test (95% confidence interval).
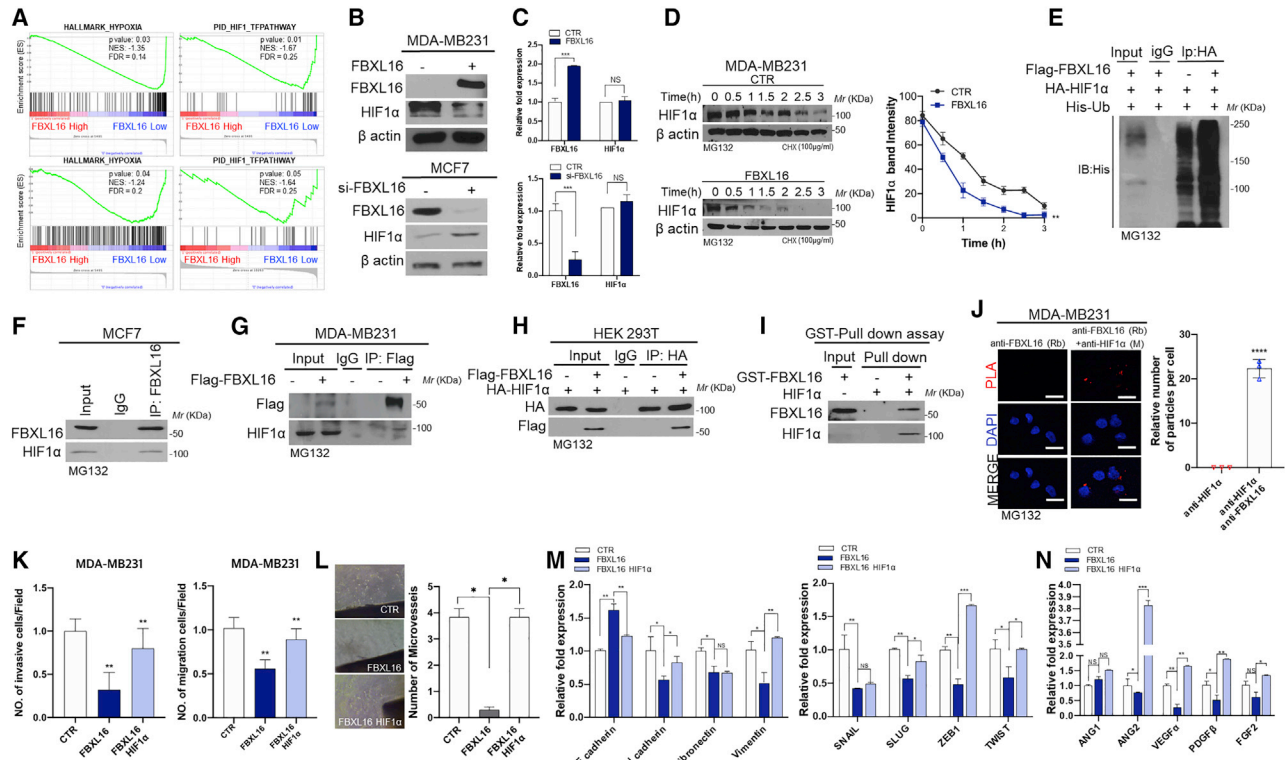
Figure 3. FBXL16 directly targets HIF1α for proteasomal degradation

(A) GSEA analysis of FBXL16-regulated hallmarks and signaling pathways using the data from GSE10810 and GSE14548 public breast cancer databases.

(B and C) Western blotting and quantitative real-time PCR analysis of FBXL16 and HIF1α protein and mRNA expression using FBXL16-overexpressing MDM-MB231 and FBXL16-silenced MCF7 cells.

(D) CHX pulse assay was performed to measure the half-life of HIF1α using MDA-MB231 cells transfected with FBXL16-overexpressing vector (left); representative graph quantifying HIF1α expression (right).

(E) Ubiquitination assay of HIF1α using the Ub-His-overexpressing HEK293T cells with or without FLAG-FBXL16 expression. Cells were treated with MG132 (10 μM) for 6 h before harvesting.

(F) Co-immunoprecipitation assay was performed, and the cell lysate was immunoprecipitated with an FBXL16 antibody or an immunoglobulin G (IgG) control.

(G) MDA-MB231 cells were transfected with Flag-FBXL16 and lysates were immunoprecipitated with FLAG antibody.

(H) HEK293T cells overexpressing vectors of Flag-FBXL16 and HA-HIF1α were co-transfected into HEK293T cells for 48 h, then harvested, and the lysate was immunoprecipitated with an HA antibody.

(I) The HA-HIF1α overexpression vector was transfected into HEK293T cells. The cell lysates were subjected to the GST pull-down assay with the indicated GST fusion proteins to pull down the FBXL16 protein.

(J) Representative images and graph of PLA-positive signal using MDA-MB231 cells fixed with primary antibodies against FBXL16 and HIF1α. The number of plots was analyzed using ImageJ software. Scale bar, 100 μm.

(K) Invasion and migration assays were performed with overexpression of FBXL16 alone or together with HIF1α in MDA-MB231 cells.

(L) Aortic ring assay was performed under the same rescue experimental conditions.

(M and N) Quantitative real-time PCR analysis was performed to check the expression of EMT markers and regulators of EMT and angiogenesis. β-actin was used as a control for normalization of expression.

Data are presented as mean of three independent experiments (SD). **p < 0.01, ***p < 0.001, n.s., not significant. All data were statistically analyzed using a t test (95% confidence interval).

Downregulation of FBXL16 through the p38/miR-135b-3p axis in TNBCs

To investigate whether an upstream regulator of FBXL16 acts to downregulate FBXL16 expression in TNBCs. We treated MDA-MB231 cells with inhibitors of the main signaling pathway to measure their effect on expression of FBXL16. Quantitative real-time PCR analysis showed that when we blocked the MAPK signaling pathway using the inhibitors of U0126 (MEK 1/2 inhibitor), a JNK inhibitor, and SB203580 (p38 MAP kinase in-hibitor), FBXL16 mRNA expression was significantly increased compared to when other signaling pathway inhibitors were used (Figure 5A). Next, we blocked the expression of p38, JNK, and EKR using siRNAs and found that the protein expression level of FBXL16 was significantly increased after blocking p38 expression in MDA-MB231 cells compared to levels seen in the other groups (Figure 5B; Figure S4A). Subsequently, we blocked p38 expression by siRNA and then treated with or without CoCl₂. We found the HIF1α expression was decreased
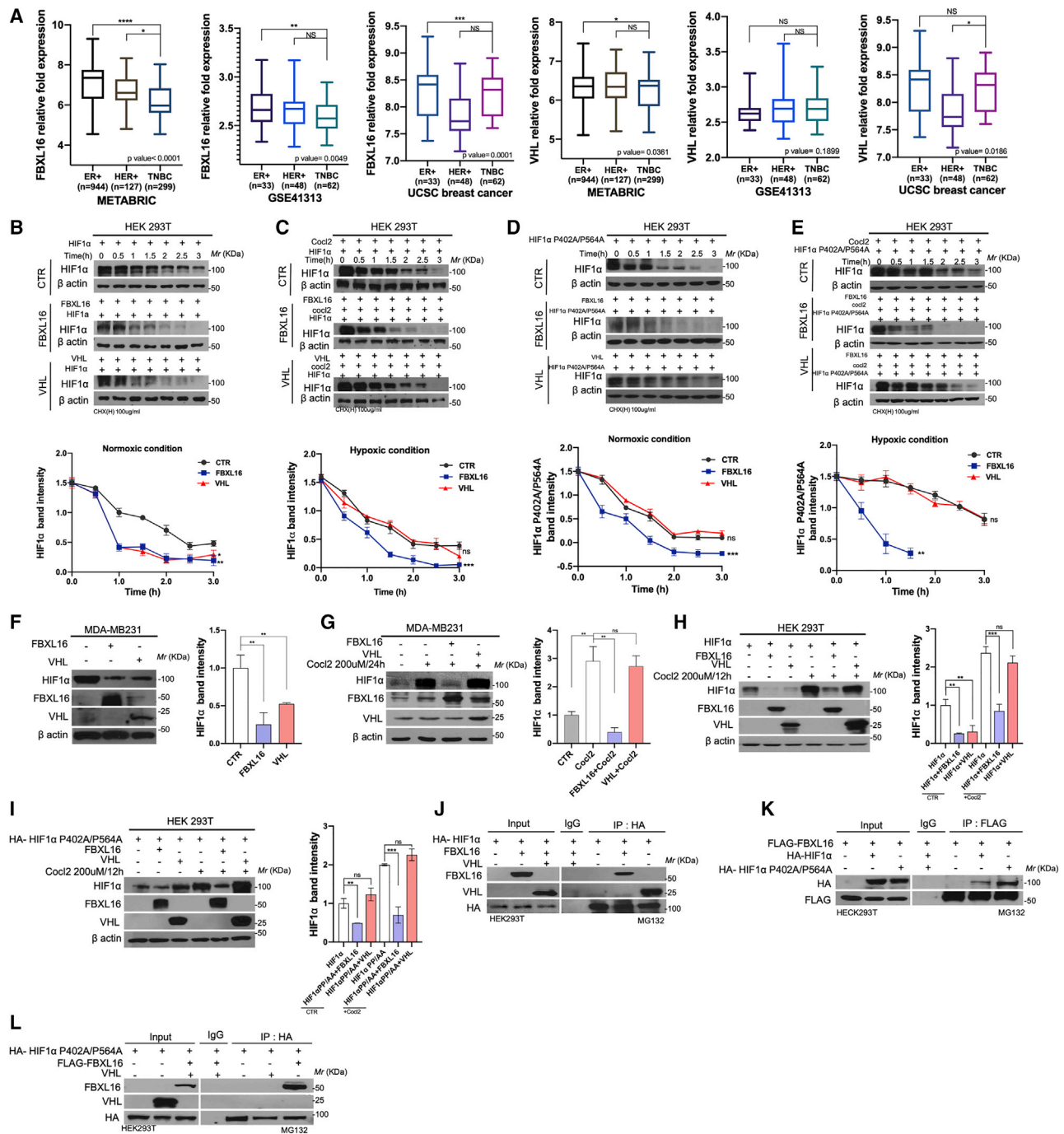
Figure 4. FBXL16 regulates HIF1α stability independent of oxygen conditions

(A) Analysis of expression of FBXL16 and VHL using the data from METABRIC, GEO datasets (GSE41313), and UCSC public breast cancer databases.

(B) The HEK293T cells were transfected with overexpressing plasmid of HIF1α with or without FBXL16 or VHL-overexpressing vector. The cells were treated with CHX (100 μg/mL) for times indicated, and the half-life of HIF1α was detected by western blot analysis, with the graph showing quantification of the blot (below).

(C) Half-life of HIF1α protein expression was measured with the treatment of CoCl₂ (200 μM) using the same conditions on HEK293T cells. The graph displays the quantification (below).

(D) The half-life of HIF1α protein was detected using the HEK293T cells transfected with plasmid expressing HIF1α P402A/P564A-overexpressing plasmid alone or together with overexpression of FBXL16 or VHL vectors. The transfected cells were treated with CHX for the times indicated, and the quantification is shown in the graph (below).

(E) Parallel experiments were performed with CoCl₂ treatment for 12 h to check the half-life of HIF1α.

(legend continued on next page)

when the p38 expression was blocked, while its expression was rescued in p38-silenced MDA-MB231 cells with the treatment of CoCl$_2$ (Figure S4B). Next, we treated MDA-MB231 cells with the SB203580 for 24 h and then transfected si-FBXL16 into the cells. The invasive /migratory and tube-formation abilities of cells were decreased following SB23580 treatment, whereas their abilities increased again after blocking FBXL16 expression in SB23580-treated MDA-MB231 cells (Figures 5C and 5D). To investigate how p38 can downregulate FBXL16 expression in TNBC cells, we hypothesized that this was caused by methylation in the promoter of FBXL16. A methylation assay was performed with p38 inhibitor treatment in MDA-MB231 cells. However, no methylation was observed in the FBXL16 promoter after blocking p38 activation (Figure S4C). Since microRNAs (miRNAs) play important roles in tumor progression by binding to specific 3′ UTRs of target mRNAs for degradation or translational repression (Bartel, 2004; Fabian et al., 2010), moreover, miRNAs can directly regulate F-box proteins (Wu and Pfeffer, 2016). To investigated whether the FBXL16 transcript level was downregulated by miRNAs in TNBCs. We screened miRNAs that have the potential to bind to the 3′ UTR of FBXL16 using public data from miRNA databases. Finally, there were nine microRNAs predicted to have binding sites in the 3′ UTR of FBXL16. Furthermore, the microRNA has-miR-135b-3p showed the highest expression level in the TNBCs compared to other miRNAs using the GSE61723 database; additionally, low expression of has-miR-135b-3p showed a better survival rate of breast cancer patients (Figure 5E; Figure S4D). Quantitative real-time PCR analysis showed that the FBXL16 expression level dramatically decreased transfected has-miR-135b-3p mimic into MCF7 cells compared to other groups (Figure 5F). The reverse results were observed in has-miR-135b-3p inhibitor-treated MDA-MB231 cells (Figure 5G). TCGA breast cancer database analysis also showed that there was a negative correlation between expression of FBXL16 and has-miR-135b-3p (Figure 5H). To further confirm that the miR-135b-3p can directly bind to the 3′ UTR of FBXL16, we performed the luciferase reporter assay using a pGL3UC luciferase reporter construct containing the 3′ UTR of FBXL16 and then transfected it into HEK293T cells along with miR-cont or miR-135b-3p. The mutant 3′ UTR of FBXL16 with a mutated binding site for miR-135b-3p was used as a negative control. The luciferase activity of cells with the wild-type 3′ UTR vector overexpressing miR-135b-3p was dramatically decreased compared to that of the cells overexpressing miR-135b-3p together with the mutant 3′ UTR vector (Figure 5I). Moreover, the HIF1α expression was suppressed when we treated the inhibitor of miR-135b-3p. However, this expression was rescued with the treatment of CoCl$_2$ and miR-135b-3p inhibitor together in MDA-MB231 cells (Figure S4E). Subsequently, the invasion, migration, and tube-formation assays showed that these capabilities decreased when we transfected miR-135b-3p inhibitor into MDA-MB231 cells as compared to the control group then rescued after blocking FBXL16 expression using miR-135b-3p inhibitor-treated MDA-MB231 cells (Figures 5J and 5K). To investigate the correlation between p38 and miR-135b-3p in regulating FBXL16 expression in TNBC, quantitative real-time PCR analysis was performed and showed that has-miR-135b-3p expression was significantly decreased after blocking p38 activation in MDA-MB231 cells (Figures 5L and 5M). Additionally, a positive correlation exists between p-p38 and has-miR-135b-3p expression in the TCGA breast cancer database (Figure 5N). Quantitative real-time PCR and western blot analysis also showed that FBXL16 expression was increased after blocking the p38 expression, while its expression was inhibited again after co-expression of miR-135b-3p in MDA-MB231 cells (Figures S4F–S4I). Overall, these results indicate that the expression of FBXL16 was downregulated by the p38/miR-135b-3p axis in TNBCs.

A negative correlation between FBXL16 and HIF1α and p-p38 protein expression is associated with poor clinical outcomes in breast cancer

To investigate the clinical importance of the above findings, we performed IHC staining using a tissue microarray (TMA) assay to determine the correlation between expression of FBXL16 and expression of HIF1α and p-p38. IHC staining showed that FBXL16 expression was negatively correlated with expression of HIF1α and p-p38, which was consistent with the above findings (Figures 6A–6D). Similarly, a negative correlation between FBXL16 and HIF1α protein expression level also was observed using the breast cancer patients' tissues from the Hanyang University hospital (Figure 6E). Moreover, the Kaplan-Meier survival analysis using these breast cancer tissues showed that high expression of FBXL16 coupled with low expression of HIF1α was associated with a better prognosis (Figure 6F). Additionally, high expression of FBXL16 coupled with low expression of miR-135b-3p or low expression both of p-p38 and miR-135b-3p revealed a high survival rate of patients using the data from TCGA database (Figures 6G and 6H). Together, these findings revealed that the expression of FBXL16 was negatively correlated with HIF1α and p-p38 expression at the protein level. Breast cancer patients with high expression of FBXL16 and low levels of HIF1α or has-miR-135b-3p expression had better survival rates. Therefore, targeting the p38/has-miR-135b-3p axis to elevate FBXL16 expression in metastatic breast cancers could provide a useful strategy for treatment of aggressive breast cancer (Figure 6I).

(F and G) MDA-MB231cells was transfected with FBXL16 or VHL-overexpressing vectors. The expression of HIF1α, FBXL16, and VHL was analyzed using western blot analysis with or without CoCl$_2$ treatment for 24 h (left). The graphs display the quantification (right).

(H and I) Similar experiments were performed using overexpression of HIF1α or HIF1α P402A/P564A mutation vectors HEK293T cells with the CoCl$_2$ treatment for 12 h. The graphs display the quantification (right).

(J) Co-IP assays were performed using HEK293T cells transfected with Ha- HIF1α vector alone or together with FBXL16 or VHL-overexpressing vectors. The cell lysates were immunoprecipitated to pull down FBXL16 and VHL protein.

(K and L) Co-IP assays indicating that FBXL16 can interact with HIF1α at different sites compared to VHL using HEK293T cells with the overexpression of HIF1α wild-type or HIF1α P402A/P564A mutation vectors. β-actin was used as a control for normalization of expression.

Data are presented as mean of three independent experiments (SD). **p < 0.01, ***p < 0.001; n.s., not significant. All data were statistically analyzed by a t test (95% confidence interval).
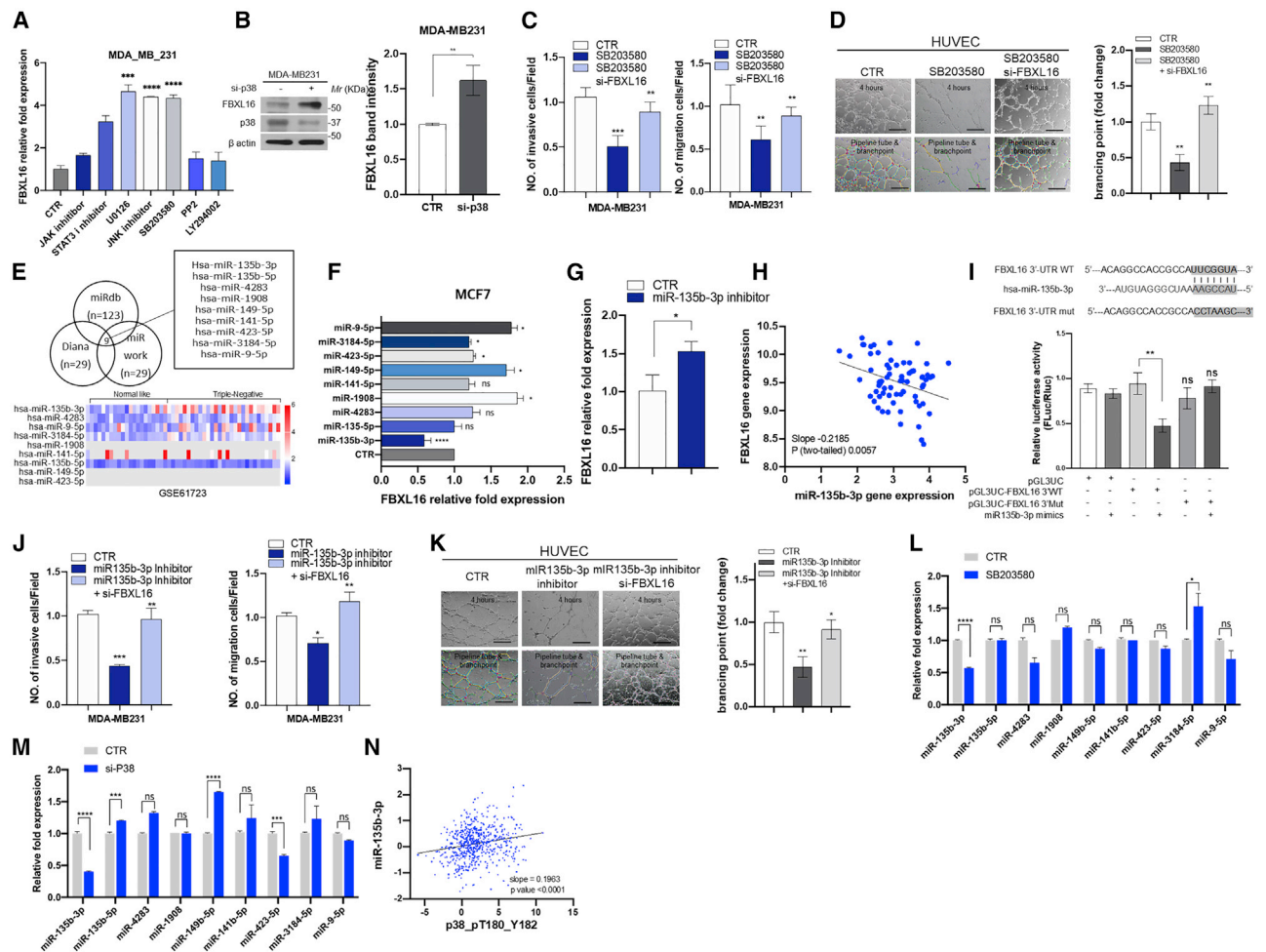
Figure 5. The expression of FBXL16 was suppressed by the p38/miR-135b-3p axis in TNBCs

(A) Quantitative real-time PCR analysis of FBXL16 mRNA expression in MDA-MB231 after treatment with appropriate inhibitors.

(B) Western blotting analysis of FBXL16 expression in p38-silenced MDA-MB231 cell.

(C and D) Invasion, migration, and tube-formation assays were performed using MDA-MB231 cells with SB203580 (p38 inhibitor) treatment alone or together with siRNA against FBXL16.

(E) Schematic representation of miRNA prediction and screening using miRNA predictive websites (miRdb, Diana, and miRwork) (top). The heatmap analysis shows expression of the selected microRNAs in luminal and basal types of breast cancer using the public data from the GSE86278 dataset. Red and blue indicate upregulation and downregulation, respectively.

(F) Quantitative real-time PCR analysis of FBXL16 mRNA expression after overexpressing these microRNA mimics in MCF7 cells.

(G) Quantitative real-time PCR analysis of FBXL16 mRNA expression in MDA-MB231 cell with the treatment of miR-135b-3p inhibitor.

(H) A negative correlation between FBXL16 and miR-135b-3p was observed using the data from TCGA breast cancer database.

(I) Graphic scheme of the miR-135b-3p binding to the 3′ UTR region of FBXL16 (top). The luciferase reporter assay was performed after wild-type (WT) FBXL16 3′ UTR and mutant FBXL16 3′ UTR co-transfection with miR-135b-3p in HEK293T cells (below).

(J and K) Invasion, migration, and HUVEC tube-formation assays were performed with the inhibitor treatment alone or together with knockdown of FBXL16 expression in MDA-MB231 cell.

(L and M) Quantitative real-time PCR analysis of miRNA expression after blocking the p38 with inhibitor or siRNA in MDA-MB231 cells. The results are represented by a heatmap. White and red indicate low and high expression, respectively.

(N) A positive correlation between FBXL16 and p38_pT180_Y182 was obtained using the data from TCGA breast cancer database. Data are presented as mean of three independent experiments (SD). **p < 0.01, ***p < 0.001; n.s., not significant. The experiments were performed at least three times. All data were statistically analyzed by a t test (95% confidence interval).

DISCUSSION

TNBCs are considered the most difficult breast cancer to cure because of the lack of expression of molecular targets ER, PR, or HER2 (Denkert et al., 2017). E3 ligases have been implicated in TNBC progression (Liu et al., 2020; Pang et al., 2019); however, the mechanisms and targets of most E3 ligases remain to be explored. In this study, we demonstrated that the E3 ligase
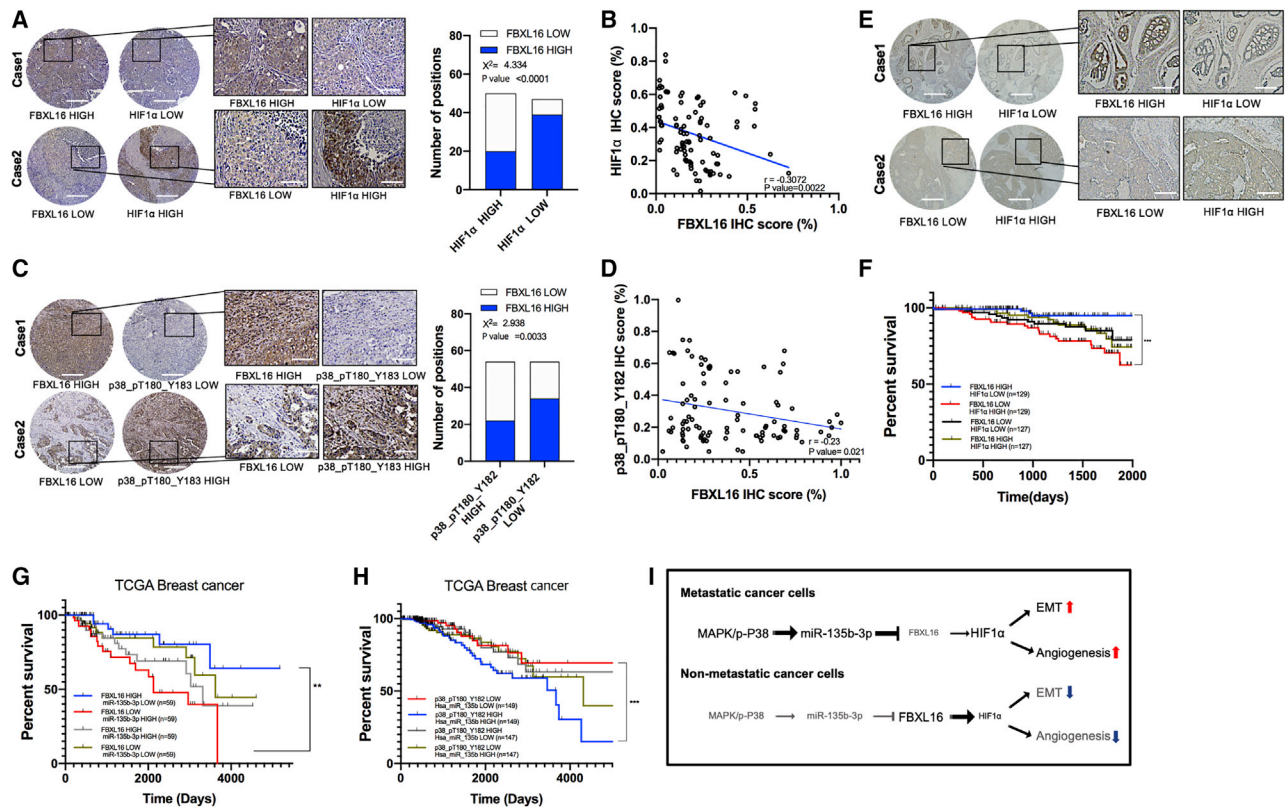
Figure 6. FBXL16 expression and HIF1α and p-p38 expression are negatively correlated in breast cancer

(A) Representative IHC staining images of FBXL16 and HIF1α expression in breast cancer tissues (left). The association between FBXL16 and HIF1α expression in breast cancer tissues was performed by χ^2 test (right).

(B) A negative correlation was observed between expression of FBXL16 and HIF1α in breast cancer tissues after analysis of IHC scores of FBXL16 and HIF1α.

(C) Representative IHC staining images of FBXL16 and p-p38 (p38_pT180_Y182) expression in breast cancer tissues (left). The association between FBXL16 and p-p38 (p38_pT180_Y182) expression in breast cancer tissues was performed by χ^2 test (right).

(D) A negative correlation was observed between FBXL16 and p-p38 (p38_pT180_Y182) protein expression in breast cancer tissues after analysis of IHC scores of FBXL16 and p-p38 (p38_pT180_Y182).

(E and F) Kaplan-Meier survival analysis showed that high expression of FBXL16 along with low expression of either of HIF1α or miR-135b-3p expression was associated with a longer survival rate of breast cancer patients using the breast cancer patients' tissues from the Hanyang University Hospital.

(G) Kaplan-Meier survival analysis showed that high expression of FBXL16 along with low expression of miR-135b-3p expression was associated with a longer survival rate of breast cancer patients using the data from human breast cancer patient tissues and TCGA breast cancer database, respectively.

(I) Schematic of p38/miR-135b-3p/FBXL16/ HIF1α axis mechanism in breast cancer.

Data are presented as mean of three independent experiments (SD). **p < 0.01, ***p < 0.001; n.s., not significant. All data were statistically analyzed by a t test (95% confidence interval).

FBXL16 can directly interact with HIF1α to regulate its ubiquitination and degradation, reducing the impact of HIF1α-mediated EMT and angiogenesis potential of breast cancer, and displaying a tumor suppressive role in regulating breast cancer progression. The p38/miR-135b axis downregulated the expression of FBXL16 in TNBCs, suggesting that targeting the p38/miR-135b axis to upregulate FBXL16 expression may be a worthwhile strategy for treatment of metastatic breast cancer.

FBPs are involved in multiple cellular processes, such as cell proliferation, invasion, angiogenesis, and metastasis, and play significant roles in regulating cancer progression (Wang et al., 2014). FBXL16 has been reported to bind to PP2A-B55α and influence the differentiation of embryonic stem cells (Honarpour et al., 2014). Additionally, FBXL16 stabilizes C-MYC by antago-

nizing the action of FBXW7, which mediates C-MYC ubiquitination and degradation (Morel et al., 2020). However, the clinical significance, functional mechanism, and/or other targets of FBXL16 in breast cancer was hitherto unclear. In this study, we found that FBXL16 can directly interact with HIF1α to regulate its ubiquitination and degradation in breast cancer. Half-life and ubiquitination assays of HIF1α showed that FBXL16 regulates HIF1α degradation and ubiquitination. Furthermore, the co-IP and PLA assays showed that FBXL16 can directly bind to HIF1α (Figures 3A–3H). Blockade of HIF1α was involved in the effects of FBXL16 on EMT and angiogenesis in breast cancer, which is consistent with the results of a previous study (Figures 3L–3N) (Muz et al., 2015; Tam et al., 2020; Tsai and Wu, 2012).

It is well known that VHL triggers hydroxylation of HIF1α in a process regulated by proline hydroxylase domain (PHD) proteins to regulate its ubiquitination and degradation under normoxic conditions (Fong and Takeda, 2008). Additionally, another study reported that FBXW7 can interact with glycogen synthase kinase 3β (GSK3β)-phosphorylated HIF1α and regulate its degradation in hypoxia (Cassavaugh et al., 2011). Here, we found that FBXL16 directly binds to HIF1α in both normoxic and hypoxic conditions to regulate its ubiquitination and stabilization. Significantly, in comparison to VHL, FBXL16 plays the more important functional role in regulating HIF1α degradation under normoxic conditions in breast cancer (Figure 4).

As reported, FBXL16 expression was upregulated by E2F1 and knockdown of FBXL16 expression induced cell proliferation in HeLa cells (Sato et al., 2010). Our data showed that FBXL16 was downregulated in metastatic breast cancer cells by p38 activation (Figures 1 and 5). Moreover, FBXL16 is expressed at low levels in TNBCs, and this is not attributable to methylation. A previous study indicated that miRNAs can function as post-transcriptional gene regulators by negatively regulating gene expression and can act to mediate cancer progression (Loh et al., 2019). In our study, we found that miR-135b-3p downregulated FBXL16 expression and showed a high expression level in the basal type of breast cancer. Additionally, assays of breast cancer patient tissue showed a negative correlation between FBXL16 and p-p38 protein expression levels. Kaplan-Meier survival analysis indicated that high expression of FBXL16 and low expression of p-p38 or miR-135b-3p resulted in a better clinical outcome. We conclude the expression of FBXL16 is downregulated by the p38/miR-135b-3p axis in metastatic breast cancer.

In this research, there are also some limitations to our study. We found that FBXL16 can directly bind to HIF1α and regulate its ubiquitination and degradation regardless of oxygen condition, and that FBXL16 binds to HIF1α at different sites from VHL. Nonetheless, we cannot define the exact binding site between FBXL16 and HIF1α. Second, the upstream regulators of the p38/miR-135b-3p axis are still unclear.

In conclusion, our study indicates that FBXL16 functions as a tumor suppressor in breast cancer progression and that the ectopic expression of FBXL16 prevents HIF1α-mediated EMT and angiogenesis in breast cancer. In TNBCs, the expression of FBXL16 was downregulated by the p38/miR-135b-3p axis, and loss of FBXL16 expression induced tumor metastasis and poor clinical outcomes in breast cancer patients. Overall, our research illustrates a novel tumor-suppressive role of FBXL16 in breast cancer and suggests that modulating the expression of FBXL16 might be a useful strategy to support metastatic breast cancer, including treatment of TNBCs.

STAR★METHODS

Detailed methods are provided in the online version of this paper and include the following:

- KEY RESOURCES TABLE
- RESOURCE AVAILABILITY
  - Lead contact
  - Material availability
  - Data and code availability
- EXPERIMENTAL MODEL AND SUBJECT DETAILS
  - Animal studies
  - Cells
- METHOD DETAILS
  - Antibodies and chemical reagents
  - Transfection
  - Cycloheximide (CHX) pulse chase assay
  - Western blot analysis
  - RNA preparation and qRT-PCR
  - Co-immunoprecipitation
  - Ubiquitination assay
  - DNA methylation analysis
  - Luciferase reporter assay
  - Glutathione S-Transferase (GST) pull-down assay
  - Cell invasion and migration assays
  - HUVECs tube formation assay
  - Aortic Ring assay
  - Immunofluorescence
  - IHC staining
  - *In situ* proximity ligation assay (PLA)
  - Human tissue microarray
  - Gene set enrichment analysis (GSEA) dataset and Kaplan-Meier analysis
- QUANTIFICATION AND STATISTICAL ANALYSIS

AUTHOR CONTRIBUTIONS

Y.-J.K. and Y.Z. conducted most of the experiments as well as contributed to manuscript preparation and data analysis. J.K.M. helped in survival data analysis. J.M.Y. helped in DNA methylation analysis. J.K.M. provided the materials and reagents for this research. S.-J.L. designed and supervised the study.

REFERENCES

Bai, C., Sen, P., Hofmann, K., Ma, L., Goebl, M., Harper, J.W., and Elledge, S.J. (1996). SKP1 connects cell cycle regulators to the ubiquitin proteolysis machinery through a novel motif, the F-box. Cell *86*, 263–274.

Bartel, D.P. (2004). MicroRNAs: genomics, biogenesis, mechanism, and function. Cell *116*, 281–297.

Bellacen, K., and Lewis, E.C. (2009). Aortic ring assay. J. Vis. Exp. 33, 1564.

Cassavaugh, J.M., Hale, S.A., Wellman, T.L., Howe, A.K., Wong, C., and Lounsbury, K. (2011). Negative regulation of HIF-1α by an FBW7-mediated degradation pathway during hypoxia. J. Cell Biochem. 112, 3882–3890.

Chen, X., Iliopoulos, D., Zhang, Q., Tang, Q., Greenblatt, M.B., Hatziapostolou, M., Lim, E., Tam, W.L., Ni, M., and Chen, Y.J.N. (2014). XBP1 promotes triple-negative breast cancer by controlling the HIF1α pathway. Nature 508, 103–107.

Clarke, C., Madden, S.F., Doolan, P., Aherne, S.T., Joyce, H., O'Driscoll, L., Gallagher, W.M., Hennessy, B.T., Moriarty, M., Crown, J., et al. (2013). Correlating transcriptional networks to breast cancer survival: a large-scale coexpression analysis. Carcinogenesis 34, 2300–2308.

DeCicco-Skinner, K.L., Henry, G.H., Cataisson, C., Tabib, T., Gwilliam, J.C., Watson, N.J., Bullwinkle, E.M., Falkenburg, L., O'Neill, R.C., and Morin, A.J.J. (2014). Endothelial cell tube formation assay for the in vitro study of angiogenesis. J. Vis. Exp. Published online September 1, 2014. https://doi.org/10.3791/51312.

Denkert, C., Liedtke, C., Tutt, A., and von Minckwitz, G.J.T.L. (2017). Molecular alterations in triple-negative breast cancer—the road to new treatment strategies. Lancet 389, 2430–2442.

Dent, R., Trudeau, M., Pritchard, K.I., Hanna, W.M., Kahn, H.K., Sawka, C.A., Lickley, L.A., Rawlinson, E., Sun, P., and Narod, S.A. (2007). Triple-negative breast cancer: clinical features and patterns of recurrence. Clin. Cancer Res. 13, 4429–4434.

Fabian, M.R., Sonenberg, N., and Filipowicz, W. (2010). Regulation of mRNA translation and stability by microRNAs. Annu. Rev. Biochem. 79, 351–379.

Fong, G.H., and Takeda, K. (2008). Role and regulation of prolyl hydroxylase domain proteins. Cell Death Differ. 15, 635–641.

Gilkes, D.M., Semenza, G.L., and Wirtz, D.J.N.R.C. (2014). Hypoxia and the extracellular matrix: drivers of tumour metastasis. Nat. Rev. Cancer 14, 430–439.

Herman, J.G., Graff, J.R., Myöhänen, S., Nelkin, B.D., and Baylin, S.B. (1996). Methylation-specific PCR: a novel PCR assay for methylation status of CpG islands. Proc. Natl. Acad. Sci. USA 93, 9821–9826.

Hon, W.-C., Wilson, M.I., Harlos, K., Claridge, T.D., Schofield, C.J., Pugh, C.W., Maxwell, P.H., Ratcliffe, P.J., Stuart, D.I., and Jones, E.Y. (2002). Structural basis for the recognition of hydroxyproline in HIF-1α by pVHL. Nature 417, 975–978.

Honarpour, N., Rose, C.M., Brumbaugh, J., Anderson, J., Graham, R.L., Sweredoski, M.J., Hess, S., Coon, J.J., and Deshaies, R.J. (2014). F-box protein FBXL16 binds PP2A-B55α and regulates differentiation of embryonic stem cells along the FLK1+ lineage. Mol. Cell Proteomics 13, 780–791.

Ivshina, A.V., George, J., Senko, O., Mow, B., Putti, T.C., Smeds, J., Lindahl, T., Pawitan, Y., Hall, P., Nordgren, H., et al. (2006). Genetic reclassification of histologic grade delineates new clinical subtypes of breast cancer. Cancer Res. 66, 10292–10301.

Jaakkola, P., Mole, D.R., Tian, Y.-M., Wilson, M.I., Gielbert, J., Gaskell, S.J., von Kriegsheim, A., Hebestreit, H.F., Mukherji, M., and Schofield, C.J.J.S. (2001). Targeting of HIF-α to the von Hippel-Lindau ubiquitylation complex by O2-regulated prolyl hydroxylation. Science 292, 468–472.

Labidi-Galy, S.I., Clauss, A., Ng, V., Duraisamy, S., Elias, K.M., Piao, H.-Y., Bilal, E., Davidowitz, R.A., Lu, Y., and Badalian-Very, G.J.O. (2015). Elafin drives poor outcome in high-grade serous ovarian cancers and basal-like breast tumors. Oncogene 34, 373–383.

Li, Y., Zou, L., Li, Q., Haibe-Kains, B., Tian, R., Li, Y., Desmedt, C., Sotiriou, C., Szallasi, Z., Iglehart, J.D., et al. (2010). Amplification of LAPTM4B and YWHAZ contributes to chemotherapy resistance and recurrence of breast cancer. Nat. Med. 16, 214–218.

Lin, A., Li, C., Xing, Z., Hu, Q., Liang, K., Han, L., Wang, C., Hawke, D.H., Wang, S., and Zhang, Y. (2016). The LINK-A lncRNA activates normoxic HIF1α signalling in triple-negative breast cancer. Nat. Cell Biol. 18, 213–224.

Liu, R., Zheng, H.-Q., Zhou, Z., Dong, J.-T., and Chen, C. (2009). KLF5 promotes breast cell survival partially through fibroblast growth factor-binding protein 1-pERK-mediated dual specificity MKP-1 protein phosphorylation and stabilization. J. Biol. Chem. 284, 16791–16798.

Liu, Z.-j., Semenza, G.L., and Zhang, H.-F. (2015). Hypoxia-inducible factor 1 and breast cancer metastasis. J. Zhejiang Univ. Sci. B. 16, 32–43.

Liu, S.-s., Qi, J., Teng, Z.-d., Tian, F.-t., Lv, X.-x., Li, K., Song, Y.-j., Xie, W.-d., and Hu, Z.-w.H. (2020). Resistomycin attenuates triple-negative breast cancer progression by inhibiting E3 ligase Pellino-1 and inducing SNAIL/SLUG degradation. Signal Transduct. Target. Ther. 5, 1–3.

Loh, H.-Y., Norman, B.P., Lai, K.-S., Rahman, N.M.A.N.A., Alitheen, N.B.M., and Osman, M.A.O. (2019). The regulatory role of MicroRNAs in breast cancer. Int. J. Mol. Sci. 20, 4940.

Ma, X.J., Dahiya, S., Richardson, E., Erlander, M., and Sgroi, D.C. (2009). Gene expression profiling of the tumor microenvironment during breast cancer progression. Breast Cancer Res. 11, R7.

Masson, N., Willam, C., Maxwell, P.H., Pugh, C.W., and Ratcliffe, P.J. (2001). Independent function of two destruction domains in hypoxia-inducible factor-α chains activated by prolyl hydroxylation. EMBO J. 20, 5197–5206.

Mathe, A., Wong-Brown, M., Morten, B., Forbes, J.F., Braye, S.G., Avery-Kiejda, K.A., and Scott, R.J. (2015). Novel genes associated with lymph node metastasis in triple negative breast cancer. Sci. Rep. 5, 15832.

Miller, L.D., Smeds, J., George, J., Vega, V.B., Vergara, L., Ploner, A., Pawitan, Y., Hall, P., Klaar, S., Liu, E.T., and Bergh, J. (2005). An expression signature for p53 status in human breast cancer predicts mutation status, transcriptional effects, and patient survival. Proc. Natl. Acad. Sci. USA 102, 13550–13555.

Montagner, M., Enzo, E., Forcato, M., Zanconato, F., Parenti, A., Rampazzo, E., Basso, G., Leo, G., Rosato, A., and Bicciato, S. (2012). SHARP1 suppresses breast cancer metastasis by promoting degradation of hypoxia-inducible factors. Nature 487, 380–384.

Morel, M., Shah, K.N., and Long, W. (2020). The F-box protein FBXL16 up-regulates the stability of C-MYC oncoprotein by antagonizing the activity of the F-box protein FBW7. J. Biol. Chem. 295, 7970–7980.

Muz, B., de la Puente, P., Azab, F., and Azab, A.K. (2015). The role of hypoxia in cancer progression, angiogenesis, metastasis, and resistance to therapy. Hypoxia 3, 83.

The Cancer Genome Atlas Network. (2012). Comprehensive molecular portraits of human breast tumours. Nature 490, 61–70.

Pang, K., Park, J., Ahn, S.G., Lee, J., Park, Y., Ooshima, A., Mizuno, S., Yamashita, S., Park, K.-S., Lee, S.-Y., et al. (2019). RNF208, an estrogen-inducible E3 ligase, targets soluble Vimentin to suppress metastasis in triple-negative breast cancers. Nat. Commun. 10, 1–13.

Pawitan, Y., Björre, J., Amler, L., Borg, A.L., Egyhazi, S., Hall, P., Han, X., Holmberg, L., Huang, F., Klaar, S., et al. (2005). Gene expression profiling spares early breast cancer patients from adjuvant therapy: derived and validated in two population-based cohorts. Breast Cancer Res. 7, 5805.

Pedraza, V., Gomez-Capilla, J.A., Escaramis, G., Gomez, C., Torné, P., Rivera, J.M., Gil, A., Araque, P., Olea, N., Estivill, X., and Fárez-Vidal, M.E. (2010). Gene expression signatures in breast cancer distinguish phenotype characteristics, histologic subtypes, and tumor invasiveness. Cancer 116, 486–496.

Polakis, P. (2001). More than one way to skin a catenin. Cell 105, 563–566.

Randle, S.J., and Laman, H. (2016). F-box protein interactions with the hallmark pathways in cancer. Semin. Cancer Biol. 36, 3–17.

Riaz, M., van Jaarsveld, M.T., Hollestelle, A., Prager-van der Smissen, W.J., Heine, A.A., Boersma, A.W., Liu, J., Helmijr, J., Ozturk, B., Smid, M., et al. (2013). miRNA expression profiling of 51 human breast cancer cell lines reveals subtype and driver mutation-specific miRNAs. Breast Cancer Res. 15, R33.

Romero-Cordoba, S.L., Rodriguez-Cuevas, S., Bautista-Pina, V., Maffuz-Aziz, A., D'Ippolito, E., Cosentino, G., Baroni, S., Iorio, M.V., and Hidalgo-Miranda, A. (2018). Loss of function of miR-342-3p results in MCT1 over-expression and contributes to oncogenic metabolic reprogramming in triple negative breast cancer. Sci. Rep. 8, 12252.

Sabatier, R., Finetti, P., Cervera, N., Lambaudie, E., Esterni, B., Mamessier, E., Tallet, A., Chabannon, C., Extra, J.M., Jacquemier, J., et al. (2011). A gene

expression signature identifies two prognostic subgroups of basal breast cancer. Breast Cancer Res. Treat. *126*, 407–420.

Sato, K., Kusama, Y., Tategu, M., and Yoshida, K. (2010). FBXL16 is a novel E2F1-regulated gene commonly upregulated in p16INK4A-and p14ARF-silenced HeLa cells. Int. J. Oncol. *36*, 479–490.

Semenza, G.L. (2012). Molecular mechanisms mediating metastasis of hypoxic breast cancer cells. Trends Mol. Med. *18*, 534–543.

Serra-Pérez, A., Planas, A.M., Núñez-O'Mara, A., Berra, E., García-Villoria, J., Ribes, A., and Santalucía, T.J.J.o.B.C. (2010). Extended ischemia prevents HIF1α degradation at reoxygenation by impairing prolyl-hydroxylation: role of Krebs cycle metabolites. 285, 18217-18224.

Silver, D.P., Richardson, A.L., Eklund, A.C., Wang, Z.C., Szallasi, Z., Li, Q., Juul, N., Leong, C.O., Calogrias, D., Buraimoh, A., et al. (2010). Efficacy of neoadjuvant Cisplatin in triple-negative breast cancer. J. Clin. Oncol. *28*, 1145–1153.

Skowyra, D., Craig, K.L., Tyers, M., Elledge, S.J., and Harper, J.W.J.C. (1997). F-box proteins are receptors that recruit phosphorylated substrates to the SCF ubiquitin-ligase complex. 91, 209–219.

Tam, S.Y., Wu, V.W., and Law, H.K.J.F.i.O. (2020). Hypoxia-Induced Epithelial-Mesenchymal Transition in Cancers: HIF-1α and Beyond. 10, 486.

Torre, L.A., Islami, F., Siegel, R.L., Ward, E.M., and Jemal, A. (2017). Global Cancer in Women: Burden and Trends (AACR).

Tripathi, V.K., Subramaniyan, S.A., and Hwang, I. (2019). Molecular and Cellular Response of Co-cultured Cells toward Cobalt Chloride ($CoCl_2$)-Induced Hypoxia. ACS Omega *4*, 20882–20893.

Tsai, Y.-P., and Wu, K.-J. (2012). Hypoxia-regulated target genes implicated in tumor metastasis. J. Biomed. Sci. *19*, 102.

Vuong, D., Simpson, P.T., Green, B., Cummings, M.C., and Lakhani, S.R. (2014). Molecular classification of breast cancer. Virchows Arch. *465*, 1–14.

Wang, Z., Liu, P., Inuzuka, H., and Wei, W. (2014). Roles of F-box proteins in cancer. Nat. Rev. Cancer *14*, 233–247.

Wu, Z.-H., and Pfeffer, L.M. (2016). MicroRNA regulation of F-box proteins and its role in cancer. Semin. Cancer Biol. *36*, 80–87.

Yang, Y., Kitagaki, J., Wang, H., Hou, D.X., and Perantoni, A. (2009). Targeting the ubiquitin-proteasome system for cancer therapy. Cancer Sci. *100*, 24–28.

Zhang, J., Zhu, L., Fang, J., Ge, Z., and Li, X. (2016). LRG1 modulates epithelial-mesenchymal transition and angiogenesis in colorectal cancer via HIF-1α activation. J. Exp. Clin. Cancer Res. *35*, 29.

STAR★METHODS

KEY RESOURCES TABLE

Reagent or resource	Source	Identifier
Antibodies		
anti-E cadherin	Abcam	Cat# ab1416
anti-SLUG	Abcam	Cat# ab27568
anti-ZEB1	Abcam	Cat# ab124512
anti-fibronectin	Abcam	Cat# ab6328
anti-vimentin	Abcam	Cat# ab8978
anti-angiogenin1	Abcam	Cat# ab8451
anti-angiogenin 2	Abcam	Cat# ab56301
anti-CD31	Abcam	Cat# ab28364
anti-PDGFβ	Abcam	Cat# ab23914
anti-HIF1α	Abcam	Cat# ab82832
anti-FBXL16	Abcam	Cat# ab133197
anti-TWIST	Santa Cruz	Cat# sc-81417
anti-FGF2	Santa Cruz	Cat# sc-1360
anti-VEGF	Santa Cruz	Cat# sc-152
anti-normal mouse IgG	Santa Cruz	Cat# sc-2025
anti-β-actin	Santa Cruz	Cat# sc-47778
anti-N-cadherin	BD Transduction Laboratories	Cat# 610920
anti-SNAIL	Cell Signaling	Cat# 3879S
anti-goat Alexa Fluor 488	GeneTex	Cat# a32814
anti-mouse Alexa Fluor 546	GeneTex	Cat# a-11030
Bacterial and virus strains		
DH5a Competent cells	Tiangen	Cat# CB101
BL21 (DE3) Competent cells	Tiangen	Cat# CB105
Chemicals, peptides, and recombinant proteins		
PEI (polyethylenimine)	Polyscience	Cat# 23966-1
Lipofectamine 2000	Thermo Fisher	Cat# 11668030
Matrigel Growth Factor Reduced Basement Membrane Matrix	Corning	Cat# 354230
LY294002	Sigma Aldrich	Cat# 154447-36-6
PP2	Sigma Aldrich	Cat# 529573
SB203580	Sigma Aldrich	Cat# 559389
U0126	Sigma Aldrich	Cat# 662005
JAK inhibitor	Sigma Aldrich	Cat# 420099
STAT3 inhibitor	Sigma Aldrich	Cat# 573097
JNK1 inhibitor	Sigma Aldrich	Cat# 420116
Cycloheximide	Calbiochem	Cat# 66819
MG132	Calbiochem	Cat# 474791
Critical commercial assays		
Power SYBR green PCR Master Mix	iinvtirogen	Cat# 4367659
Pierce GST Protein Interaction Pull-Down Kit	Thermo Fisher	Cat# 21516
Deposited data		
RNA-seq	Pawitan et al., 2005	GSE1456
RNA-seq	Li et al., 2010	GSE19615

(Continued on next page)

Continued

Reagent or resource	Source	Identifier
RNA-seq	Clarke et al., 2013	GSE42568
RNA-seq	Sabatier et al., 2011	GSE216532
RNA-seq	Ivshina et al., 2006	GSE4922
RNA-seq	Pedraza et al., 2010	GSE10810
RNA-seq	Riaz et al., 2013	GSE41313
RNA-seq	Miller et al., 2005	GSE3494
RNA-seq	Silver et al., 2010	GSE18864
RNA-seq	Mathe et al., 2015	GSE61723
RNA-seq	Ma et al., 2009	GSE14548
RNA-seq	Romero-Cordoba et al., 2018	GSE86278
Experimental models: Cell lines		
MDA-MB231	the Korean Cell Line Bank (KCLB)	Cat# 30026
MCF7	the Korean Cell Line Bank (KCLB)	Cat# 30022
HEK293T	American Type Culture Collection (ATCC)	Cat# CRL 1573
MCF10A	American Type Culture Collection (ATCC)	Cat# CRL 10317
HUVEC	American Type Culture Collection (ATCC)	Cat# PCS 100 013
T47D	the Korean Cell Line Bank (KCLB)	Cat# 30133
MDA-MB-453	the Korean Cell Line Bank (KCLB)	Cat# 30131
SKBR3	the Korean Cell Line Bank (KCLB)	Cat# 30030
Experimental models: Organisms/strains		
NOD/SCID mice	Central Lab Animal Inc., Seoul, Korea	Mouse inbred stains
Oligonucleotides		
FBXL16-Human PCR expression (5′-3′) GTGCTGTACCAGCCCAAGTT	This study	N/A
HIF1α-Human PCR expression (5′-3′) GAAAGCGCAAGTCCTCAAAG	This study	N/A
Recombinant DNA		
FBXL16	Origene	Cat# RC206362
VHL	Origene	Cat# RC216151
HIF1α vector	Addgene	Cat# 18949
Software and algorithms		
ImageJ	Open source	https://imagej.nih.gov/ij/
GraphPad Prism	Graphpad	https://www.graphpad.com/scientific-software/prism/
Nikon NIS-element Advanced Research	Nikon	https://www.microscope.healthcare.nikon.com/products/software/nis-elements

RESOURCE AVAILABILITY

Lead contact
Further information and requests for resources and reagents should be directed to and will be fulfilled by the lead contact, Su-Jae Lee (sj0420@hanyang.ac.kr)

Material availability
Plasmids and reagents generated in this study are available on request.

Data and code availability
Additional datasets used for this study were obtained from the following studies: GSE1456 (Pawitan et al., 2005), GSE19615 (Li et al., 2010), GSE42568 (Clarke et al., 2013), GSE216532 (Sabatier et al., 2011), GSE4922 (Ivshina et al., 2006), GSE10810 (Pedraza et al.,

2010), GSE41313 (Riaz et al., 2013), GSE3494 (Miller et al., 2005), GSE18864 (Silver et al., 2010), GSE61723 (Mathe et al., 2015), GSE14548 (Ma et al., 2009) and GSE86278 (Romero-Cordoba et al., 2018). No novel code was written for the analysis of the dataset.

EXPERIMENTAL MODEL AND SUBJECT DETAILS

Animal studies
All animal experiments were performed according to the guidelines of the Institutional Animal Care and Use Committee of Academia Sinica. The NOD/SCID mice used in this study were obtained from Orient Bio (Central Lab Animal Inc., Seoul, Korea). Six-week-old female NOD/SCID mice with a similar weight were randomized into two experimental groups (LM1 control group and FBXL16-LM1 group; each group n = 6). A total of 40 μL (1x10^6 cells) of LM1 control cells or FBXL16-overexpressing LM1 cells were injected into the fat pad of the mice. After injection, the tumor volume of each mouse was measured using a digital caliper. The mice were then sacrificed for subsequent experiments 5 weeks after injection. Tumor volumes were determined by measuring the length (l) and width (w) and using the following formula: volume = shortest diameter^2 × longest diameter/2.

Cells
MDA-MB231 and MCF7 breast cancer cell lines were obtained from the Korean Cell Line Bank (KCLB). HEK293T, MCF10A, and HUVEC cells were obtained from the American Type Culture Collection (ATCC). MDA-MB231 and HEK293T cell lines were cultured in Dulbecco's modified Eagle's medium, MCF7 cells were grown in Roswell Park Memorial Institute medium from GIBCO (Grand Island, NY, USA) with 10% fetal bovine serum in the presence of penicillin (100 U/mL) and streptomycin (100 μg/mL). MCF10A cell lines were incubated in Dulbecco's modified Eagle's medium/F12 supplemented with 100 ng/ml cholera toxin, 500 ng/ml hydrocortisone, 20 ng/ml epidermal growth factor (EGF), 10 mg/ml insulin, L-glutamine, and 5% horse serum. HUVECs were cultured in EGM-2 media (Lonza, Clonetics, CC-4176) with appropriate growth factors. For the chamber experiments, the transfected cells were incubated under standard conditions for 48 h, then transferred to a chamber incubator (Forma Scientific, Anaerobic System Model 1029) supplemented with 1% O_2, 5% CO_2, and N_2 balance for 4 h or 16 h, and then harvested for subsequent experiments.

METHOD DETAILS

Antibodies and chemical reagents
LY294002 (#154447-36-6, a PI3K inhibitor), PP2 (#529573, an SRC inhibitor), SB203580 (#559389, a P38 inhibitor), U0126 (#662005, an ERK1/2 inhibitor), JNK1 inhibitor, JAK inhibitor (#420099), and STAT3 inhibitor were purchased from Sigma Aldrich (St Louis, MO, USA). Cycloheximide (CHX, #66819) and MG132 (#474791, proteasome inhibitor) were purchased from Calbiochem (LaJolla, CA, USA). Antibodies against E cadherin (ab1416), SLUG (ab27568), ZEB1 (ab124512), fibronectin (ab6328), vimentin (ab8978), angiogenin1 (ANG1, ab8451), angiogenin 2 (ANG2, ab56301), CD31 (ab28364), PDGFβ (ab23914), HIF1α (ab82832), and FBXL16 (ab133197) were purchased from Abcam (Cambridge, UK). TWIST (sc-81417), FGF2 (sc-1360), VEGF (sc-152), normal mouse IgG (sc-2025), and β-actin (sc-47778) antibodies were obtained from Santa Cruz Biotechnology (Santa Cruz, CA, USA). N-cadherin (610920) and SNAIL (3879S) antibodies were purchased from BD Transduction Laboratories (St. Louis, MO, USA) and Cell Signaling (Beverly, MA, USA), respectively. Goat IgG antibody (HRP), rabbit IgG antibody (HRP), and mouse IgG antibody (HRP) were obtained from GeneTex (Irvine, CA, USA). Anti-goat Alexa Fluor 488 and anti-mouse Alexa Fluor 546 antibodies were purchased from Invitrogen (Carlsbad, CA, USA). The vectors of FBXL16 (#RC206362) and VHL (#RC216151) were purchased from Origene (Rockville, MD, USA); the HIF1α vector (#18949) was obtained from Addgene (Watertown, MA, USA).

Transfection
Cells were transfected with DNA vector or siRNAs using polyethylenimine (PEI) or LipofectamineTM 2000 (Invitrogen) according to the manufacturer's instructions. All siRNAs were purchased from Genolution Pharmaceuticals (Seoul, Korea). All experiments were repeated at least three times.

Cycloheximide (CHX) pulse chase assay
The siRNAs or DNA vector were transfected into cells for 48 h and then treated with 100 μg/mL of cycloheximide (Sigma Aldrich, USA) for the indicated times. Proteins were collected and analyzed by western blotting. The CHX experiment was performed according to a previous report (Liu et al., 2009).

Western blot analysis
Cells were lysed in lysis buffer [40 mM Tris-HCl (pH 8.0), 120 mM NaCl, 0.1% Nonidet-P40] supplemented with protease inhibitors. Proteins were separated by SDS-PAGE and transferred to a nitrocellulose membrane (Amersham, Arlington Heights, IL, USA). The membrane was probed with the indicated primary antibody and developed with a peroxidase-conjugated secondary antibody. The proteins were visualized by enhanced chemiluminescence (ECL) (Amersham, IL, USA) according to the manufacturer's instructions.

RNA preparation and qRT-PCR

Total RNA was isolated using TRIzol (Invitrogen, Carlsbad, CA, USA). Real-time quantitative PCR was performed using the KAPA SYBR FAST qPCR kit from KAPA Biosystems (Wilmington, MA, USA), according to the manufacturer's instructions. All analyses were performed using a Rotor Gene Q (QIAGEN, Hilden, Germany) PCR cycler. mRNA expression levels were normalized to the expression of beta-actin. Results were expressed as fold change calculated using the ΔΔCt method relative to the control samples. β-actin served as an internal normalization control. All primers were purchased from DNA Macrogen (Seoul, Korea).

Co-immunoprecipitation

The transfected cells were treated with 10 μM MG132 (EMD Millipore, Burlington, MA, USA) for 6 h before harvest. Cell pellets were lysed buffer [40 mM Tris-HCl (pH 8.0), 120 mM NaCl, 0.1% Nonidet-P40] supplemented with protease inhibitors. Lysates were cleared by centrifugation at 12,000 rpm at 4°C for 30 min. Protein concentration was measured using bovine serum albumin as standards (Pierce, Rockford, IL, USA). For immunoprecipitation, lysates were incubated with the appropriate primary antibody at 4°C overnight on a rotator. The next day, 10 μL of Protein A-agarose beads (Santa Cruz Biotechnology, Santa Cruz, CA, USA) were added to each sample and samples were incubated at 4°C for 2 h. The immunocomplexes were washed with 1x cold PBS three times. The immunoprecipitates were analyzed by western blotting.

Ubiquitination assay

Ubiquitination assay was performed using denaturing immunoprecipitation (IP). Specifically, the His-Ub plasmid, Flag-FBXL16, and HA-HIF1α vectors were transfected into HEK293T cells and incubated for 48 h, then treated with 10 μM MG132 for 6 h to inhibit proteasomal degradation before harvesting the cells for subsequent experiments. Lysis buffer [denatured IP buffer: Tris–HCl (40 mM, pH 8.0), NaCl (120 mM), Nonidet-P40 (0.1%)] was used to lyse the cells, and the IP buffer containing anti-HA tag antibody was used to precipitate the HIF1α protein.

DNA methylation analysis

For methylation analysis, a standard phenol-chloroform method was used to extract genomic DNA. A total of 1 μg of DNA was modified by bisulfite using the EZ DNA Methylation Kit (Zymo Research, Orange, CA, USA), which guarantees a > 99% conversion rate of nonmethylated C nucleotides to U and for protection of methylated cytosine residues. Methylation-specific PCR (MSP) primer pairs, located close to the putative transcription start site in the 5 CpG island, were used to analyze gene promoter methylation. A total of 2 μL of bisulfite-treated DNA was used as a template, and the JumpStart REDTaq DNA Polymerase (Sigma-Aldrich Co.) was used for the amplification reaction. The protocol was used as previously described(Herman et al., 1996). MSP primers were as follows: FBXL16 Unmethylation Forward-1 5′-TTTAGGAGATTTTAGGATAGGGTGT-3′ and Reverse-1 5′-ACTAAAAACTAAAAACAACAAC AAC-3′; Unmethylation Forward-2 5′- TTTTAAGTGGTGGTTAAGGGTTG-3′ and Reverse-2 5′-AAAAAAAACAAAAAAACAAACACC-3′; Methylation Forward-1 5′-TTTTTTAGGAGATTTTAGGATAGGGC-3′ and Reverse-1 5′- AACTAAAAACTAAAAACGACGACGA-3′; Methylation Forward-2 5′-TTTTTAAGTGGTGGTTAAGGGTC-3′, and Reverse-2 5′-AAAAAAAACGAAAAAACAAACG-3′. The amplified products were resolved by 1% agarose gel electrophoresis, stained with ethidium bromide, and photographed under UV illumination.

Luciferase reporter assay

Luciferase reporter assays were performed using vectors encoding putative target sites in the 3′ untranslated region (UTR). HEK293T cells were seeded into 60 mm dishes when after reaching approximately 50% confluency and were then cotransfected with reporter plasmid (1 μg), pRL-CMV-Renilla (Promega, Madison, WI) plasmid (1 μg) and miRNA using Plus reagent and Lipofectamine (Invitrogen) for 48 h. Luciferase activity was measured using a dual-luciferase reporter assay system (Promega) following the manufacturer's instructions and normalized to Renilla luciferase activity. All constructs were verified by sequencing. All experiments were performed in triplicate.

Glutathione S-Transferase (GST) pull-down assay

The GST pull-down assay was performed as previously described (Polakis, 2001). The coding sequence of FBXL16 was cloned into the vector pGEX-4T-1 to obtain the GST tag protein. The tag-fusion protein was purified according to the standard protocol (Pierce GST Protein Interaction Pull-Down Kit, #21516) and the concentration of the protein was measured using the Thermo Scientific[TM] BCA protein Assay kit (# 23227). Mammalian cells were incubated to 80% confluence and were harvested with Pull-Down Lysis Buffer (Thermo Scientific, #1858601) on ice for approximately 30 min and centrifuged (12,000 × g at 4°C) for 30 min. Then, the cell lysates were incubated with GST or GST-FBXL16 protein overnight at 4°C. Subsequently, GST-beads were added to capture the GST-fusion protein. The proteins were then washed and eluted with the appropriate buffer and analyzed by western blotting.

Cell invasion and migration assays

For the invasion assay, the filter inserts were coated with 10 mg/mL growth factor-reduced Matrigel (BD Biosciences, CA, USA) and incubated at 37°C for at least 30 min. Then, the cells in serum-starved medium were seeded into the coated filter inserts (Corning, NY, USA). The outside wells were filled with 10% FBS-containing medium. After incubation for 48 h at 37°C, non-invading cells in the inner

surface of the chamber were removed with a cotton swab. Invasive cells on the outer surface of the chamber were fixed and stained using Diff-Quick kit (Fisher Scientific, Pittsburgh, PA, USA) and photographed. The migration assay was similar to the invasion assay, except that the filter inserts were not coated with Matrigel. The invasive and migrated cells were determined by counting the cells in five microscopic fields per well. The extent of invasion and migration was expressed as the average number of cells per field. All experiments were performed three times.

HUVECs tube formation assay
For the tube formation assay, cells were prepared according to the standard protocol (DeCicco-Skinner et al., 2014). Briefly, HUVECs were added to 24-well plates coated with growth factor-reduced Matrigel (BD Bioscience, CA, USA). Breast cancer cells with or without DNA vector transfection were incubated in the upper side of the chamber. Tube formation was examined under a phase-contrast microscopic observation at the indicated time. The tube formation analysis was performed using ImageJ software (NIH, Bethesda, MD, USA) as previously described. All experiments were performed three times.

Aortic Ring assay
C57BL mice (6–7 weeks old) were used for the aortic ring assay. The assay was performed according to the manufacturer's instructions (Bellacen and Lewis, 2009). Briefly, the mouse thoracic aorta was excised, and all extraneous fat, tissue, and adventitia were removed. The aorta ring was then cut to approximately 1mm in length. Each ring was embedded in a basement matrix extract (BME) dome. The transfected cells were seeded into the upper inserts with EBM medium (GIBCO, Carlsbad, CA) supplemented with 2% FBS, 50 U/mL penicillin, and 50 μg/mL streptomycin (Cellgro; Corning, NY, USA). The sprouting was observed and photographed under a stereomicroscope over a period of 6–12 days.

Immunofluorescence
Transfected cells were fixed with 4% paraformaldehyde and permeabilized with 0.1% Triton x-100 in phosphate-buffered saline (PBS). Blocking was with blocking buffer (5% goat serum and 2% BSA in 1X PBS) for at least 30 min at RT. The cells were then incubated at 4°C with appropriate primary antibody overnight. The next day, the cells were washed three times in phosphate-buffered saline with 0.05% Tween 20 (PBST). Stained proteins were set with Alexa Fluor 488- or 594-conjugated anti-rabbit or anti-mouse secondary antibodies (Molecular Probes, Seoul, Korea). Nuclei were counterstained with 4′,6-diamidino-2-phenylindole (DAPI; Sigma, St. Louis, MO, USA). Cells were observed using an Olympus Ix71 fluorescence microscope (Olympus, Seoul, Korea).

IHC staining
Mouse tissues were fixed in formalin for the preparation of paraffin sections. Paraffin-embedded tissue sections were deparaffinized in xylene, and rinsed with 100, 95, 80, and 70% ethanol, followed by flowing water. Epitopes were washed with 20 mg/mL protein kinase K in PBS with 0.1% Triton-x-100. Sections were stained with H&E or immunostained with primary antibody at 4°C overnight. After washing with PBS, biotinylated goat anti-rabbit IgG or anti-mouse IgG antibody was applied to the sections. After washing with PBS, the ABC reagent (Vector Laboratories, Burlingame, CA, USA) was applied to the sections. Color reaction was performed with 3,3′-diaminobenzidine (Vector Laboratories), stained with hematoxylin, and cleared with 70, 80, 95, and 100% ethanol and xylene. The sections were mounted with Canada balsam. Images were captured using a DP71 digital imaging system on an IX71 microscope (Olympus, Seoul, Korea).

In situ proximity ligation assay (PLA)
Cells on coverslips were fixed with 4% paraformaldehyde and permeabilized with 0.1% Triton x-100 in phosphate buffered saline (PBS). The cells were then incubated overnight with anti-FBXL16 (1:200) and anti-HIF1α (1:200) primary antibodies at 4°C. The next day, fixed cells were washed three times in phosphate-buffered saline with 0.05% Tween 20 (PBST). *In situ* PLA was performed according to the manufacturer's protocol using a Duolink Detection Kit (Sigma) and detected using the relative secondary antibodies. Following ligation and amplification of the PLA probes with the corresponding buffer, coverslips were then washed twice with 1x Duolink II wash buffer B and finally washed with 0.01% Duolink II wash buffer B (diluted in high purity buffer). Nuclei were counterstained with DAPI (Sigma Aldrich). Cells were observed using an Olympus 1x71 fluorescence microscope (Olympus, Seoul, Korea)

Human tissue microarray
BR1902 and HBreD140Su07 human breast cancer tissue microarray samples were obtained from US Biomax (Rockville, MD, USA). Human breast cancer patients' tissues (Hanyang University Hospital, Seoul, Korea). These samples were examined by a pathologist. Images were captured using a DP71 digital imaging system on an IX71 microscope (Olympus, Tokyo, Japan).

Gene set enrichment analysis (GSEA) dataset and Kaplan-Meier analysis
Previously published microarray data of GSE1456, GSE19615, GSE42568, GSE216532, GSE4922, GSE41313, GSE3494, GSE18864, GSE61723, GSE14548, GSE86278 and GSE10810 were used for reanalysis. Gene signatures obtained by comparing

gene sets from either the Molecular Signature Database (MSigDB) database or published gene signatures were analyzed using GSEA analysis. The KM plot program (http://kmplot.com/analysis/) was used to analyze the survival data, as previously described (Labidi-Galy et al., 2015).

QUANTIFICATION AND STATISTICAL ANALYSIS

All experiments were repeated at least three times, and the data are reported as mean ± standard deviation (SD, represented by error bars). χ^2 test was used to measure the gene expression association of breast cancer patient tissues. Survival curves were conducted using the Kapan-Meier method and the difference between groups was assessed by the Log-rank (Mantal-Cox) test. All statistical analyses were conducted with two-tailed parametric Student's t tests or analysis of variance for multivariate analysis in GraphPad Prism software 7.0 (GraphPad, Inc., La Jolla, CA, USA). The variance was similar between groups, and the significance was defined as $*p < 0.05$, $**p < 0.01$, and $***p < 0.001$ compared to controls. Non significance was denoted as n.s.